



ELSEVIER

Available online at www.sciencedirect.com

SCIENCE @ DIRECT®

Nuclear Instruments and Methods in Physics Research A 545 (2005) 97–113

NUCLEAR
INSTRUMENTS
& METHODS
IN PHYSICS
RESEARCH
Section A

www.elsevier.com/locate/nima

Conceptual design of an improved CMS RPC Muon Trigger using the Hadron Outer scintillators

C. Albajar^{a,1}, J.F. de Trocóniz^{a,*,1}, J. Rohlf^b, G. Wrochna^{c,2}

^a*Departamento de Física Teórica C-XI, Universidad Autónoma de Madrid, E28049 - Madrid, Spain*

^b*Boston University, Boston, MA, USA*

^c*Soltan Institute for Nuclear Studies, Warsaw, Poland*

Received 12 November 2004; accepted 17 January 2005

Available online 25 March 2005

Abstract

Hadron Outer (HO) scintillators located around the CMS coil are sensitive to muons. They can be used in coincidence with RPC chambers for the Muon Trigger. This paper contains a brief description of the two systems and the proposal of how they can be integrated. Backgrounds, efficiencies, and trigger rates have been calculated. The conclusion is that rate reduction factors as high as 100 can be obtained for ~90% efficiency.

© 2005 Elsevier B.V. All rights reserved.

PACS: 29.40.Cs; 29.40.Mc

Keywords: LHC; CMS; Resistive plate chambers; Hadron calorimeter; Muon trigger

1. Introduction

The muon spectrometer for the CMS detector is realized by instrumenting the return iron yoke for the solenoidal magnet. The yoke is configured as four iron disks on each end and five cylindrical wheels in between. Layers of drift tube chambers

(DT) for tracking and triggering, and resistive plate chambers (RPC) for additional triggering are inserted into the gaps between the layers of iron.

A layer of scintillators is also deployed around the coil to form the outer section of the hadron calorimeter (HO) providing sensitivity to late developing showers and to muons. Fig. 1 displays a transversal view of a central wheel of the CMS detector, showing the location of the Muon Barrel (MB) and HO systems.

In this paper the possibility of incorporating the information of the HO sub-detector in the RPC muon trigger is investigated in detail. The principal

*Corresponding author. Tel.: +34 91 497 3881; fax: +34 91 497 3936.

E-mail address: jorge.troconiz@uam.es (J.F. de Trocóniz).

¹Supported by CICYT under grant FPA2002-02552.

²Partially supported by the Polish Committee for Scientific Research under grant KBN 621/E-78/SPUB/P-03/DZ 5/99.

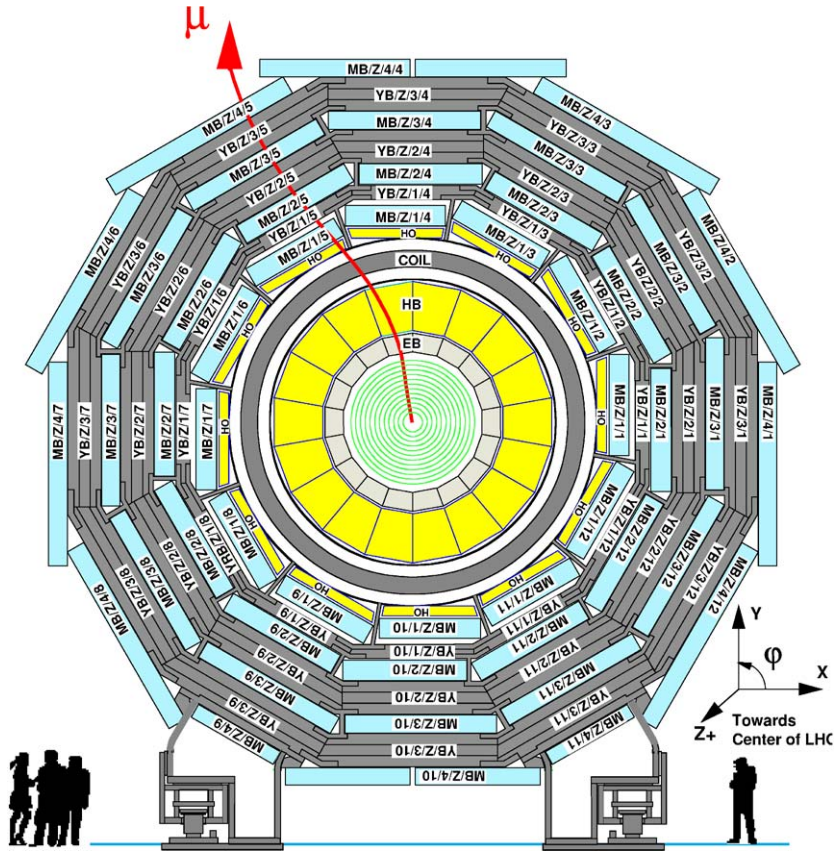


Fig. 1. Transversal view of a central wheel of the CMS detector. The location of the Muon Barrel (MB) and Hadron Outer (HO) systems, relevant for the present paper, can be observed.

motivation for this study is the golden rule for muon triggers at hadron colliders: a possible backup reduction factor should never be neglected. Experience tells that even if the trigger system works perfectly now, and the extra reduction factor is not needed yet, one cannot exclude that it will be needed later (for instance at larger luminosities). A good example is the CDF muon triggers during Run 1. To tame the muon rates it was necessary to incorporate into the algorithm, some confirmation from the hadron calorimeter in a way very much similar to the one discussed here.

At CMS an important concern is that, currently, real data on important noise sources such as the neutron background are not available. The current estimations can only be taken seriously at the

order of magnitude level. At CDF, the calculation of this kind of background was too low by a factor of about 3. A first important reason to include the HO in the RPC trigger is, therefore, to be prepared for the unexpected. Incorporating the HO would be necessary for at least another reason: it provides an important extra plane in the regions where only 4 or 3 RPC planes are available.

The HO and the RPC systems complement each other because the RPC region with the greatest noise and fewest planes is at high η , where muons give a larger signal in the HO due to the crossing angle. The second noisiest RPC trigger towers are at small η , where the HO has two layers of scintillators.

The trigger rate also grows spectacularly for low- p_T thresholds, and again the reason is related

to the number of RPC planes available. Since the muon has not enough energy to go through the full muon system, only 4 of the 6 planes can be used to form the trigger. It is clear that the additional plane provided by the HO can be essential to reduce the low- p_T threshold as much as possible. In the worst of the cases, a HO requirement is clearly better than a pre-scale: even inefficiently, the former will cut more on the background, whereas a pre-scale cuts always the same proportion of signal and background events.

The paper is organized in the following way: the HO system and the RPC trigger system are explained in Sections 2 and 3, respectively. The performance of the HO to trigger muons and its sensitivity to all relevant backgrounds affecting its occupancy are described in Section 4. The geometrical integration or mapping of the HO and the RPC systems is discussed in Section 5. The optimal trigger algorithm, and corresponding potential in terms of efficiency and rate reduction of the combined system RPC+HO are established in Section 6. Finally, the principal lines of the hardware implementation are depicted in Section

7. Section 8 summarizes the most important results.

2. HO scintillators

The standard reference for the HO detector is the HCAL TDR [1]. Only the most relevant characteristics for this study are summarized here.

The detector is made of 10 mm Bicron (BC-408) scintillator plates located between the coil and the inner RPC in Station MB1 (behind about 10 interaction lengths of material). There are two layers of scintillator in Wheel 0 (tiles $-4:4$), separated by a 15 cm iron slab. In Wheels ± 1 , ± 2 (tiles $-15:-5$, and $5:15$) there is only one layer. Tiles in a 30° sector of the same wheel are packaged together into a single mechanical unit called a tray. Trays are physically attached to the iron in front of MB1 detectors. The HO covers the full MB system (barrel+overlap regions). From the RPC trigger point of view, trigger towers up to ± 9 are covered ($|\eta| < 1.24$). Fig. 2 shows one 30° half-sector (positive pseudorapidity, tiles 1:15) of

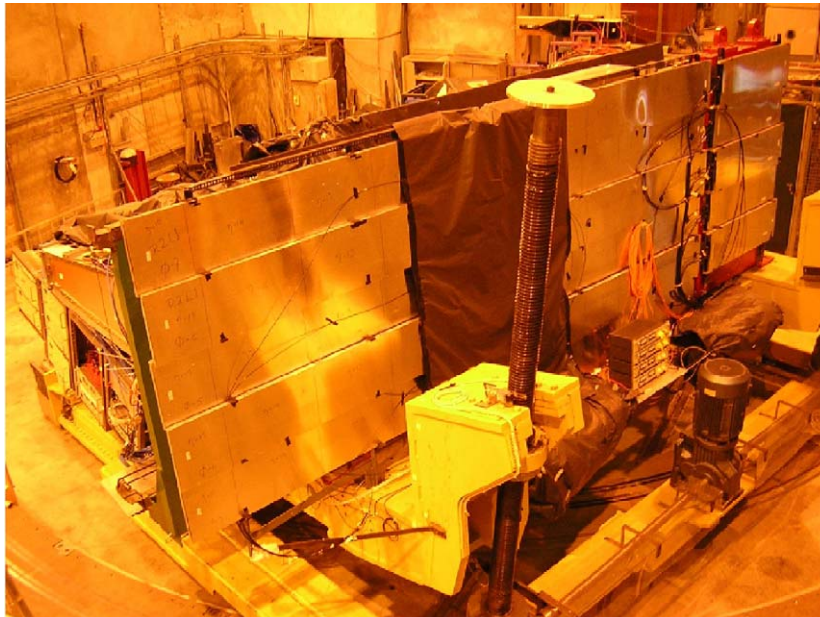


Fig. 2. One 30° half-sector (positive pseudorapidity, tiles 1:15) of the HO detector located at CERN H2 testbeam area.

the HO detector located at CERN H2 testbeam area.

The HO granularity matches the corresponding Hadron Calorimeter tower size. Tiles are 0.087×0.087 in $\eta-\phi$, which corresponds to about 50 cm (η) \times 40 cm (ϕ). There are 6 HO tiles in every MB sector. One tile corresponds to 16 RPC strips in ϕ . Therefore, in this direction, the granularity of the two detectors agree pretty well. In the longitudinal (η) direction the situation is different. An efficient map matching both detectors has been worked out in Section 5.

The readout uses Wave-Length Shifting (WLS) optical fibers embedded in a sigma type groove. There are four sigma grooves per tile. The fiber coming out of the sigma groove is spliced to a clear fiber. The clear fibers take the signal up to readout boxes where they are read by Hybrid Photo Diodes (HPD) operated at a gain of typically 2500. The output of the HPDs is integrated in windows of 25 ns (bucket). Several successive time samples are combined for energy and time measurement. The phase of the HO readout (energy vs. time) may be adjusted independently of the rest of the HCAL to yield the best signal-to-background ratio for the RPC trigger. For appropriate phase definition, 90% of the HO deposited energy is contained in two consecutive time samples.

2.1. Test beam results

The actual performance of the HO system (Wheel 1) has been measured at the 2002 test beam at CERN. The results indicate that muons at normal incidence produce 6 photo-electrons (pe) per scintillator layer. A pedestal noise of 0.9 pe/bucket (one Gaussian sigma) can be achieved [2]. These measurements have been repeated in 2003 and 2004 with final electronics. The results in the following sections will demonstrate that this performance will be adequate to significantly enhance the RPC trigger.

In this paper we use the 6 pe/mip (minimum ionization particle) and 0.9 pe noise/bucket as a reference. In an early phase of this study we used 8 pe/mip and 1.5 pe noise/bucket. The two sets of numbers produce essentially identical

results for the signal distributions. As far as the same HO energy thresholds are considered the results about efficiencies are unchanged. The important difference is in the noise occupancy levels. For the same HO energy thresholds, the corresponding rate reduction factors are different as will be discussed in Section 6.2.

3. RPC Muon Trigger

3.1. RPC system layout

The layout of the RPC chambers is shown schematically in Fig. 3. The CMS barrel consists of four muon stations, denoted by RB1, RB2, RB3, and RB4. Stations RB1 and RB2 are equipped with two (double gap) RPC layers each. Stations RB3 and RB4 contain only one RPC layer. There are also four endcap muon stations, called RE1, RE2, RE3, and RE4. Each endcap station is equipped with one RPC plane. The RE2 station is planned to be upgraded with a second RPC layer.

The physical segmentation of RPC strips in the barrel is projective in ϕ and z . RPCs in each wheel are divided in 3 along z in the so-called reference plane and in 2 in other planes. The reference plane in the barrel is RB2. In the endcaps the RPC segmentation is projective in ϕ and r . The reference plane is RE2. The strips are $\Delta\phi = (5^\circ/16^\circ)$ wide (approximately in the barrel, exactly in the endcaps).

The logical segmentation of the RPC trigger is projective in ϕ and η . It is defined by the strips in the reference plane, i.e. RB2 and RE2. In ϕ the trigger is divided into 12 sectors, 30° each. It is important to note the difference between physical detector sectors and logical trigger sectors (Fig. 4). The physical sectors are defined by the shape of the magnet yoke. They have boundaries at $15^\circ + n \times 30^\circ$ and they are centered at $n \times 30^\circ$. The logical trigger sectors have boundaries at $-5^\circ + n \times 30^\circ$ and they are centered at $10^\circ + n \times 30^\circ$. This difference is introduced to minimize the number of optical fibers transmitting the data from RPC chambers to the trigger logic. One fiber sends data from one

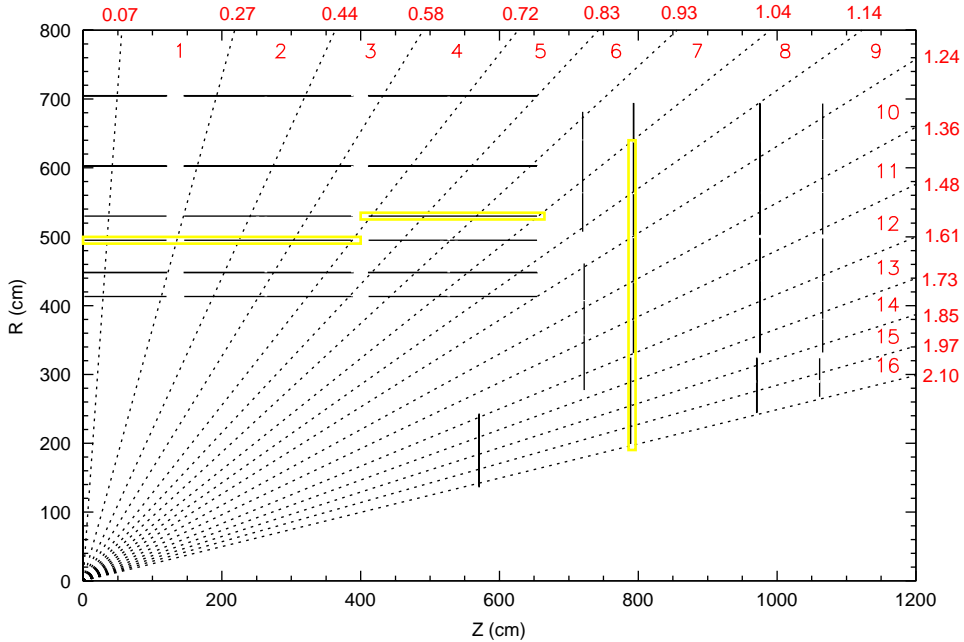


Fig. 3. Physical segmentation of RPC chambers and logical segmentation of the RPC trigger. Trigger towers (numbered from 0 to 16) and their boundaries in η are indicated.

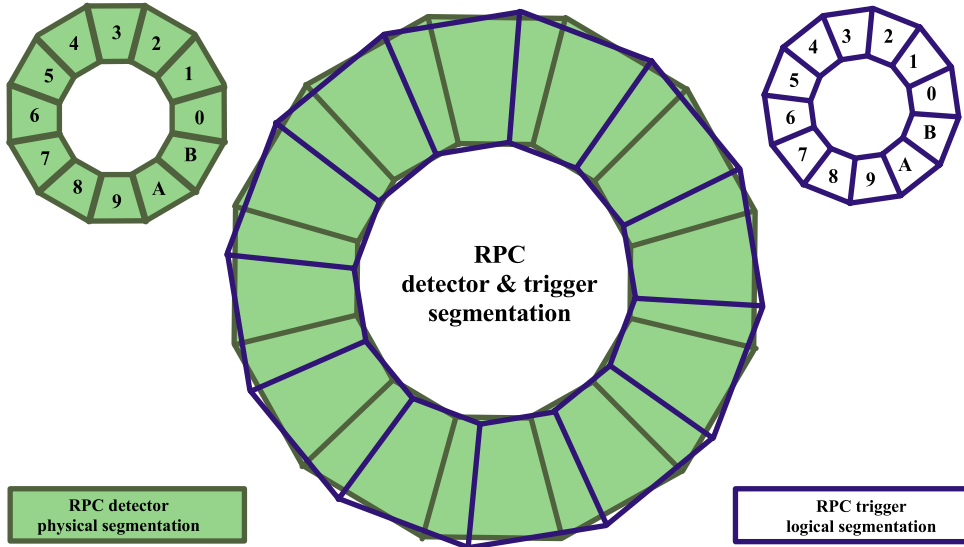


Fig. 4. Physical segmentation of RPC chambers and logical segmentation of RPC trigger in ϕ .

physical sector. The trigger logic of one sector needs data from neighboring channels to account for track bending. If the logical trigger sectors were matched to the physical ones, each trigger

sector would need fibers from three physical sectors. Thanks to the shift, only two physical sectors need to be connected to one logical trigger sector.

The segmentation in η is shown in Fig. 3. There are 33 η trigger towers numbered from -16 to 16 . Typical tower size is about 0.1η units. More details of the RPC geometry can be found in Ref. [3].

3.2. RPC Trigger principle

The principle of the RPC Trigger [4] is illustrated in Fig. 5. The solenoidal field bends tracks in the $r-\phi$ plane. A pattern of hits recorded by RPCs carries the information about the bending and can be used to determine the transverse momentum (p_T) of the track. This is done by comparison with a predefined set of patterns corresponding to various p_T^{cut} . Therefore this device is called PAttern Comparator Trigger (PACT).

The current baseline algorithm requires coincidences in a minimum number of hit planes. This minimum number depends on the trigger tower number and p_T^{cut} , as detailed in Table 1.

Up to four highest p_T muons in the barrel and four in the endcaps are selected and sent to the Global Muon Trigger (GMT). The information about number of hit planes (“trigger quality”) is sent to the GMT together with measured p_T and can be used for further selection.

3.3. RPC trigger performance

Table 2 summarizes the RPC trigger efficiencies (for 95% chamber efficiency) and trigger rates for muons with $p_T > 10 \text{ GeV}/c$ (for $50 \text{ Hz}/\text{cm}^2$ chamber noise and nominal neutron background levels),

Table 1

Minimum number of planes, over the total, for coincidences in the current RPC baseline algorithm, as a function of the trigger tower number and p_T^{cut}

	p_T range (GeV/c)	RPC trigger towers				
		0–5	6–7	8	9	10–16
Number of planes		6	5	4	3	4
Very-low- p_T	< 8	3/4	3/4	3/4	3/3	3/4
Low- p_T	8–18	4/6	4/5	3/4	3/3	3/4
High- p_T	> 18	4/6	4/5	3/4	3/3	3/4

Table 2

RPC trigger efficiencies (for 95% chamber efficiency) and trigger rates for muons with $p_T > 10 \text{ GeV}/c$ (for $50 \text{ Hz}/\text{cm}^2$ chamber noise and nominal neutron background levels), as a function of the RPC trigger tower number. The statistical MC error of the efficiency numbers is ± 0.001

RPC tower	$\epsilon(\text{RPC})$	PAC	Trigger rate (Hz)
0	0.971		
1	0.814		
2	0.832	4/6	120 ± 40
3	0.891		
4	0.886		
5	0.838		
6	0.723	4/5	13 ± 13
7	0.836		
8	0.895	3/4	1370 ± 140
9	0.745	3/3	120 ± 40

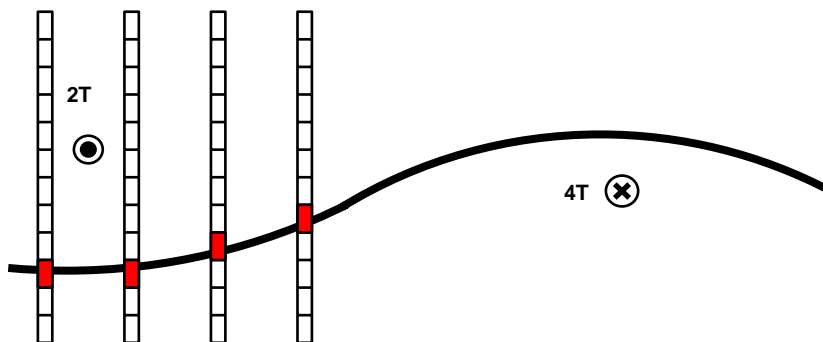


Fig. 5. RPC Pattern Comparator Trigger principle.

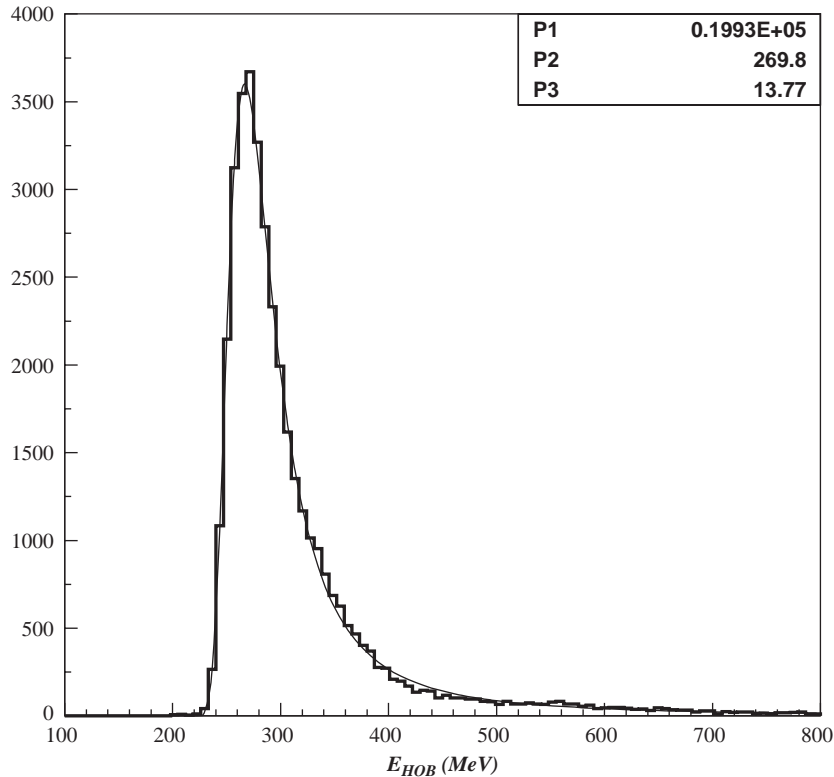


Fig. 6. The HO reconstructed energy for 100 GeV/ c p_T muons at normal incidence simulated with CMSIM123. The shape of the signal is compared to a Landau distribution and the parameters of the fit (normalization, peak energy and width) are given. In particular a peak energy of 270 MeV is found.

as a function of the RPC trigger tower number. Those numbers are taken from Ref. [5]. The rates depend strongly on the RPC trigger tower number as it can be seen. In particular, the combined rate in towers 8 and 9 (where only 4 and 3 RPC planes are used, respectively) represents 92% of the total barrel plus overlap region ($|\eta| < 1.24$). In contrast, the geometrical acceptance of towers 8 and 9 is only 16% of the total. Reduction of the rate in these two towers should be considered a priority.

4. HO performance

In this section we determine the performance of the HO detector for muons and estimate all relevant background sources.

4.1. Signal response and electronic noise occupancy

The HO tile response to muons was calculated using CMSIM123 [6]. Muons with $p_T = 100$ GeV/ c and with a flat distribution in ϕ and η were simulated.³ Fig. 6 shows the HO reconstructed energy for 100 GeV/ c muons at normal incidence. The shape of the signal is compared to a Landau distribution and the parameters of the fit given. In particular a peak reconstructed energy of 270 MeV is found. The average reconstructed energy is 310 MeV. As part of the Hadron

³To test a possible dependence on the transverse momentum, the exercise was repeated with 10 GeV/ c p_T muons. All results, and in particular the map acceptances (Section 5) and trigger efficiencies (Section 6.1), were found consistent with the ones obtained for 100 GeV/ c p_T muons.

Calorimeter, the HO energy is calibrated to account for energy deposition in non-active material. The deposited-to-reconstructed scale factor is 150. Considering this scale factor, the peak (average) deposited energy is 1.8 (2.1) MeV. Another sample of muons with $p_T = 10 \text{ GeV}/c$ was generated to check that there was no dependence on the transverse momentum of the muons.

The geometrical acceptance for muons with $|\eta| < 1.24$, defined as the proportion of muons with $E_{HO} > 0$ is 0.932 ± 0.001 , due to the gaps between wheels and wedges. The geometrical HO acceptance is, however, largely correlated to the RPC trigger acceptance, especially at Station 1, as it will be seen in Section 5.

According to the results of Section 2.1, 6 pe/mip are assigned to the peak energy at normal

incidence. The corresponding photostatistic Poisson fluctuations, and a Gaussian electronic noise with a sigma of 0.9 pe/bucket were added on top of the CMSIM energy value. The noise is evaluated, as the signal, using two buckets. A correction factor for 90% signal collection in two buckets is applied later. No ADC quantization has been implemented as it is expected that the binning should be established after deciding the trigger cut.

Fig. 7 shows the HO reconstructed energy distribution after the inclusion of photostatistics and pedestal noise effects. The full distribution is for pure noise. The sigma of the noise distribution is 64 MeV. The vertical line, at $E_{HO} = 150 \text{ MeV}$, represents the cut at 1% noise occupancy. The dotted distribution is for 100 GeV/c p_T muons in Wheel 0 (2 scintillator layers). The dashed one is for 100 GeV/c p_T muons in Wheels $\pm 1, \pm 2$. The

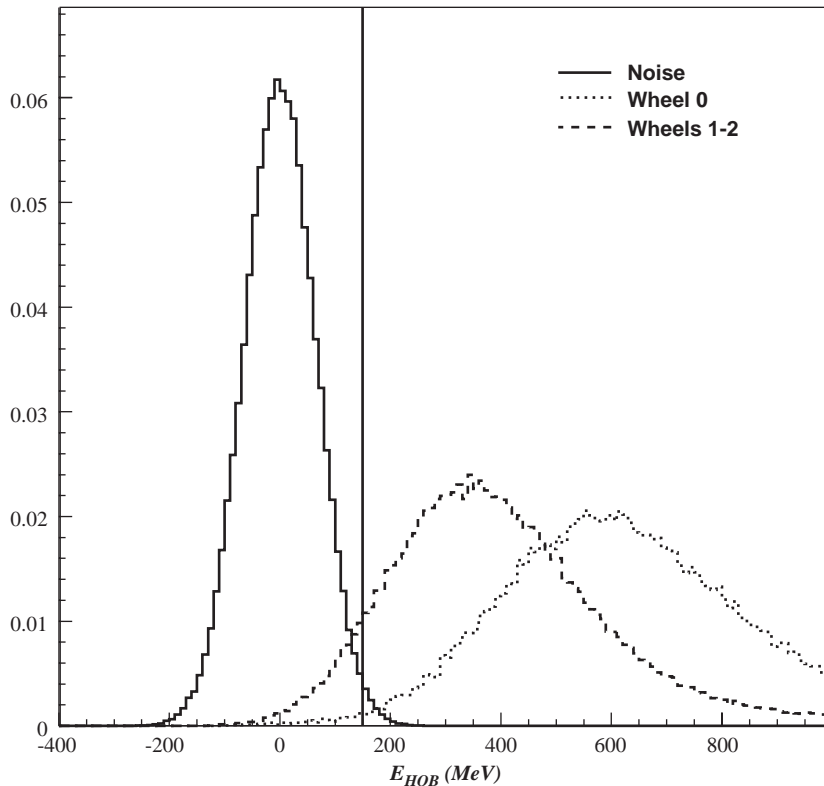


Fig. 7. The HO reconstructed energy for 6 pe/mip and 0.9 pe/bucket pedestal noise. The full distribution is for pure noise. The dotted one is for 100 GeV/c p_T muons in Wheel 0 (2 scintillator layers), including pedestal noise and photostatistics. The dashed one is for 100 GeV/c p_T muons in Wheels $\pm 1, \pm 2$. The vertical line at $E_{HO} = 150 \text{ MeV}$ represents the cut at 1% noise occupancy.

Table 3

Comparison of the noise and efficiency of the RPC and HO detectors for several HO energy thresholds, corresponding to 1%, 0.1%, and 0.01% tile occupancy levels, respectively

	Area (cm ²)	Noise (kHz)	Noise (Hz/cm ²)	Efficiency (%)
RPC	250	1.2	5	95–98
$E_{\text{HO}} > 150 \text{ MeV}$	2000	400	200	95
$E_{\text{HO}} > 200 \text{ MeV}$	2000	40	20	91
$E_{\text{HO}} > 245 \text{ MeV}$	2000	4	2	86

Note that the detector areas actually change with position. The numbers given here are an approximate average value.

width of the signal distributions is dominated by the photostatistics.

Table 3 shows a comparison of the noise and efficiency of the RPC and HO detectors. The HO parameters have been calculated for several energy thresholds, corresponding to 1%, 0.1%, and 0.01% tile occupancy levels, respectively. The same HO energy thresholds, in the case of 1.5 pe noise/bucket, correspond to 3%, 1%, and 0.1% occupancy, respectively. Note that the detector areas actually change with pseudorapidity. The numbers given in Table 3 are an approximate average value. The HO efficiency as a function of the energy threshold for fiducial muons ($E_{\text{HO}} > 0$) is also given.

4.2. Physics background occupancy

4.2.1. p – p interactions

The occupancy level in p – p interactions was calculated using minimum bias events (PYTHIA [7], including standard multiple parton interactions) simulated using CMSIM121 [6]. Both the Geisha [8] and FLUKA [9] packages were used to simulate the interaction of hadrons in the calorimeter. The average $p_{\text{T}}^{\text{hard}}$ of the events producing a HO signal is 15 GeV/ c . The dominant mechanism producing the signals is interacting punch-through (especially in the case of FLUKA).

Table 4 summarizes the HO occupancy levels for $E_{\text{HO}} > 150 \text{ MeV}$. A pile-up of 20 collisions per bunch crossing has been added, corresponding to $\mathcal{L} = 10^{34} \text{ cm}^{-2} \text{ s}^{-1}$. Even if there is a factor 5 of disagreement between both simulations the con-

Table 4

HO occupancy levels in PYTHIA minimum bias events for $E_{\text{HO}} > 150 \text{ MeV}$

	GEISHA	FLUKA
Simulated events	221k	79k
HO occupancy (Hz/cm ²)	0.33 ± 0.02	1.56 ± 0.07

A pile-up of 20 collisions per bunch crossing has been added, corresponding to $\mathcal{L} = 10^{34} \text{ cm}^{-2} \text{ s}^{-1}$. Both the GEISHA and FLUKA packages have been used to simulate the interaction of hadrons in the calorimeter.

clusion is that this rate will be negligible anyway compared to the electronic noise (Table 3).

4.2.2. Neutron-induced noise

There are two sources of neutron-induced noise. The first one is, as in the case of the muon DT and RPC chambers, the conversion background. We estimate the conversion background using the corresponding result at MB1 discussed in the Muon TDR [3]. The rate changes with pseudorapidity but is always smaller than 10 Hz/cm².

The second source, specific of proton-rich organic materials, is n – p elastic collisions, followed by proton dE/dx . Fig. 8 shows the neutron cross-section in hydrogen (from Ref. [10]). For neutrons with kinetic energy $E > 0.1 \text{ MeV}$ only the elastic cross-section matters. Using the numbers in Fig. 8 the mean free path for 1 MeV neutrons in the HO scintillator is 2.2 cm (compared to 1 cm of scintillator thickness). Therefore this background is relevant.

In order to estimate this background pions with a transverse momentum of 20 GeV/ c and a flat distribution in η and ϕ were generated with CMSIM123. All neutrons with kinetic energy larger than 1 MeV traversing the HO detectors were followed. The neutrons traversing the HO stopped there or exited unchanged. Conservatively all energy lost in the scintillators was assumed to be deposited by the scatter proton (via dE/dx).

Fig. 9 shows the total and stopped neutron fluxes (arbitrary units) at HO as a function of the incoming kinetic energy, for neutrons with $E > 1 \text{ MeV}$. The stopped flux is interpreted as the result of a neutron–proton elastic interaction. The

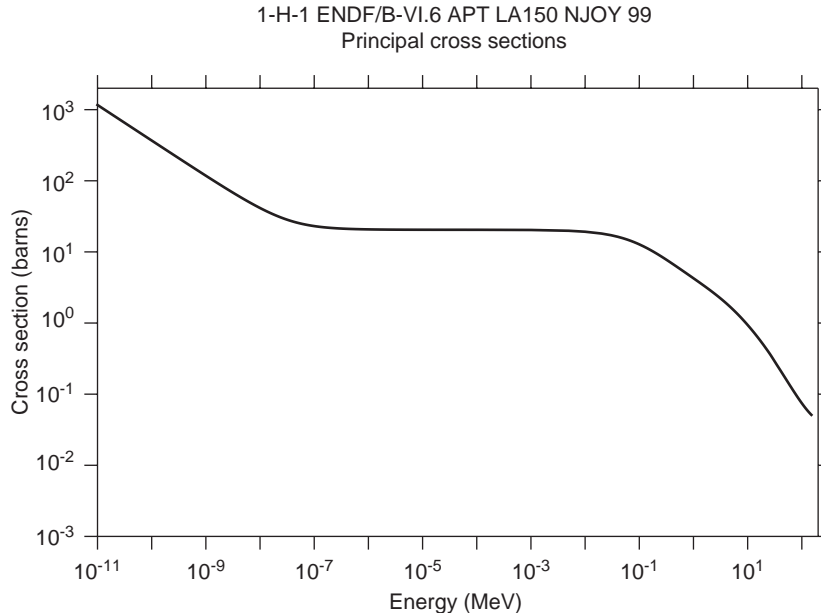


Fig. 8. Elastic neutron–proton cross-section as a function of the neutron incoming energy (from Ref. [10]). Note that in the 0.1–10 MeV range the cross-section goes down by approximately one order of magnitude.

shape of the total flux matches well the distribution in Fig. 10.6.4 of the Muon TDR [3] for MB1, including the dip around 10 MeV. The simulation was used to calculate the fraction of neutrons producing HO hits. The normalization rate was obtained from Fig. 10.6.4 in the Muon TDR (conservatively $<250 \text{ Hz/cm}^2$ for $E > 1 \text{ MeV}$ at any part of the detector).

Since the n – p elastic cross-section changes rapidly as the neutron kinetic energy decreases, special attention should be paid to the energy cut. In Fig. 8, from a plateau at $E = 0.1 \text{ MeV}$, the cross-section decreases a factor 3 (10, 100) for $E = 1$ (10, 100) MeV. The chosen value is 1 MeV since, as discussed in Section 4.1, the lowest trigger threshold considered, 150 MeV, corresponds to 1 MeV of deposited energy. This is however an overestimate, because even when the neutron stops completely in the plastic, the detected energy is smaller than its original kinetic energy. The two main reasons for this are:

- in the elastic collision not all the neutron kinetic energy is transferred to the proton;

- the proton energy deposition is much localized in space, and therefore, the reconstructed energy is strongly reduced by Birk’s law.

Therefore the calculation is rather conservative. Fig. 10 shows the effective neutron–proton cross-section as a function of the neutron incoming energy, calculated under the assumption that all stopped neutrons have been scattered elastically by the protons in the HO scintillator. The agreement with the numbers in Fig. 8 is good.

Multiplying the fraction of stopped neutrons by the Muon TDR normalization, the total neutron rate should be smaller than 25 Hz/cm^2 . For HO tiles 1–4 (Wheel 0), the fact that the HO has two scintillator layers is compensated by a smaller neutron flux.

Adding both sources, the total background rate is of the order of 35 Hz/cm^2 . Comparing the total occupancy from physical backgrounds to the electronic noise rate, it is desirable to consider a threshold so that electronic noise dominates, and the occupancy levels stay

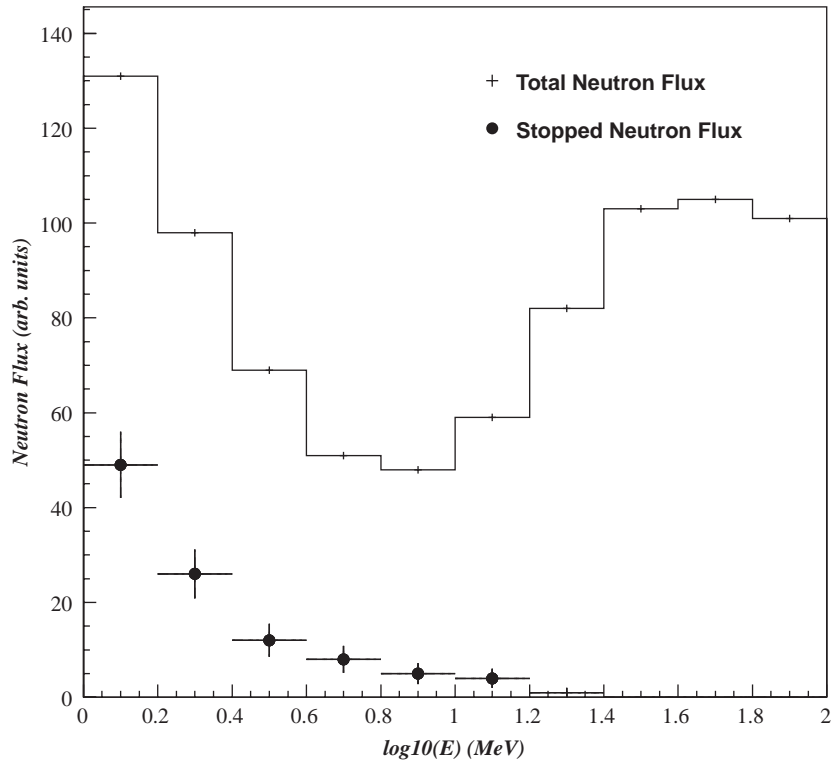


Fig. 9. The total and stopped neutron fluxes (arbitrary units) at HO as a function of the neutron incoming kinetic energy, obtained for 20 GeV/ c p_T pions simulated with CMSIM123.

under control. From Table 3 it is shown that a threshold of 150 MeV (1% noise occupancy) is appropriate.

5. Mapping of HO and RPC trigger towers

In this section the map connecting HO tiles to RPC trigger towers, necessary for the detailed specification of the trigger and its hardware implementation, is established.

Muons with $p_T = 100$ GeV/ c were simulated with CMSIM123, and the number of hit planes for every RPC trigger tower was counted. A RPC tower triggers if the number of hits is larger or equal than 4 (3) in towers 0–7 (8–9). If several RPC towers trigger, the one with best quality (number of planes) is considered. In case that two towers

with the same number of planes trigger, both of them are considered.⁴

The simulation used in this study differs from the ORCA [11] implementation in that in ORCA, as in the real PACT, not all patterns are considered. For simplicity, only the patterns providing an accumulated efficiency of at least 95% (in practice often larger) are taken into account. In this study all patterns are considered. Nevertheless, since all the numbers calculated for this paper are relative fractions this will not affect the result.

The geometric acceptance for RPC triggers with the addition of the HO has been recomputed. We find this acceptance to be 0.960 ± 0.001 ,

⁴An interesting feature of using the HO is that these data may be used to solve the ambiguity in these cases.

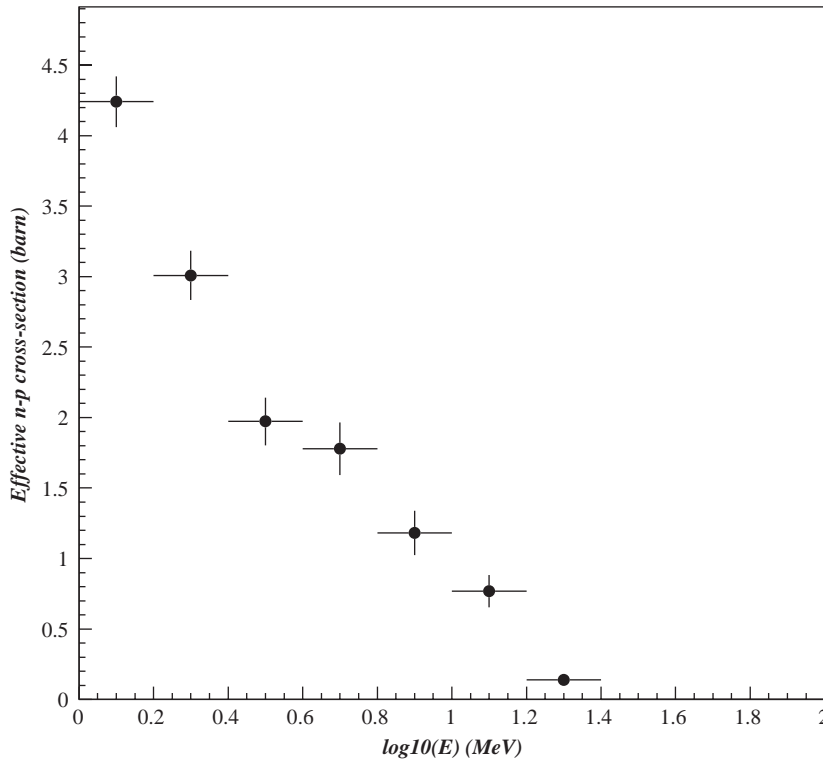


Fig. 10. The effective neutron–proton cross-section as a function of the neutron incoming kinetic energy, calculated under the assumption that all stopped neutrons have been scattered elastically by the protons in the HO scintillator.

evidencing the geometrical correlation between the HO and RPC (especially at Station 1).

We have worked out a detailed HO mapping for RPC triggers including tiles with $E_{\text{HO}} > 150$ MeV. As discussed in Section 2, in the ϕ direction the granularity of the two detectors agree well, and only one tile has been considered. Two maps in η have been computed. The first one is designed to have an acceptance larger than 99% (Safe Map). The second one is a simplified version of the former, with an acceptance of 90% in the worst case, actually larger in general (Minimal Map). There are three reasons to consider this simplified map. The first one is suitability for hardware implementation. Second, since the trigger bits of several tiles in a group are ORed and the total electronic noise grows with the total number of tiles, this number should be kept as small as possible. Third, the η information provided by the HO is more helpful if the tile

overlap between adjacent RPC trigger towers is minimized.

Table 5(left) shows the HO rapidity Safe Map, as a function of the RPC trigger tower number. Typically 3 tiles/tower have to be included, the only exceptions are Tower 0 (5 tiles), and Towers ± 5 (2 tiles). The acceptance is defined as the fraction of RPC+HO triggers, where the triggering tile ($E_{\text{HO}} > 150$ MeV) belongs to the map. In Table 5 the acceptances are first presented when the HO confirmation is required for all RPC triggers. All numbers are well above 99%. Since the proposed algorithm (Section 6) will require confirmation only for low-quality RPC triggers, Table 5 also shows the corresponding acceptances for these cases. Still all numbers are larger than 99%.

The previous numbers can be compared to the ones obtained with the Minimal Map. Table 5 (right) shows the HO rapidity Minimal Map, as a function of the RPC trigger tower number. The

Table 5
The HO rapidity Safe (left) and Minimal (right) Maps, as a function of the RPC trigger tower number

RPC tower	Safe Map			Minimal Map		
	Tiles	All triggers	Low-quality	Tiles	All triggers	Low-quality
0	–2–2	0.999	0.999	–1–1	0.988	0.985
1	1–3	0.999	0.999	2–3	0.933	0.969
2	4–6	0.999	0.998	4–5	0.982	0.987
3	5–7	0.999	0.999	6–7	0.971	0.932
4	7–9	0.999	0.998	7–8	0.915	0.913
5	9–10	0.992	0.988	9–10	0.992	0.988
6	9–11	0.999	0.999	10–11	0.992	0.992
7	11–13	0.997	0.997	11–12	0.991	0.981
8	12–14	0.995	0.991	12–13	0.918	0.870
9	13–15	0.997	0.997	14–15	0.974	0.974

The corresponding acceptances are presented for two cases: all RPC triggers and only low-quality RPC triggers. The acceptance is the fraction of RPC+HO triggers where the triggering tile ($E_{\text{HO}} > 150 \text{ MeV}$) belongs to the map. The statistical MC error of the acceptance numbers is ± 0.001 .

Minimal Map structure is simpler: now only 2 tiles/tower are included, except for Tower 0 (3 tiles). Tile overlap has been also reduced significantly. The acceptances for the Minimal Map are indeed larger than 90% (except for the case of Tower 8 and low-quality RPC triggers). In fact they are often much larger than 90%.

6. Trigger algorithm

The proposed algorithm requires HO confirmation for low-quality RPC triggers. The definition of low-quality triggers depends on the trigger tower number and the muon transverse momentum as follows:

- 3-hits for very-low- p_{T} triggers;
- 4-hits in towers 0–7 for low- and high- p_{T} triggers;
- 3-hits in towers 8–9 for low- and high- p_{T} triggers.

Effectively the HO is treated as another RPC plane, and the number of required coincidences is increased by one unit.

Tiles should provide one energy-over-threshold trigger bit. Trigger bits are ORed within the groups specified in the HO-RPC η Map. In this study no

optimization of the energy threshold as a function of position is attempted. On the contrary, a single energy threshold for all tiles is considered. Nevertheless, this optimization can be important at CMS, taking advantage of the strong η dependence of the light yield (particularly at Wheel 0) and neutron-induced background levels [3].

6.1. Efficiency

In this section the HO confirmation efficiency for RPC triggers as a function of the trigger tower number is computed. A comparison of the HO requirement efficiencies for $p_{\text{T}} = 100 \text{ GeV}/c$ muons triggered by the RPC, and for the Safe and Minimal HO-RPC rapidity maps is shown in Table 6. The HO tile energy threshold is 150 MeV (including pedestal noise and photostatistic effects). HO tile trigger bits are ORed appropriately. As can be observed, the low-quality-only requirement improves the efficiency in the most difficult cases, i.e., at the wheel separation gaps. This is clear especially at Tower 2, but also at Tower 6 (as expected from Fig. 3). Except in these two cases all efficiencies are well above 90%, often much above.

As discussed in Section 5 these efficiencies are relative, the denominator is events-satisfying-the-RPC-trigger. In order to compute absolute efficiencies (for produced muons), the numbers in

Table 6

Comparison of the HO confirmation efficiencies for 100 GeV/ c muons triggered by the RPC as a function of the RPC trigger tower number, and for the safe and minimal HO rapidity maps

RPC tower	All triggers		Low-quality	
	Safe Map	Minimal Map	Safe Map	Minimal Map
0	0.956	0.945	0.964	0.964
1	0.975	0.914	0.981	0.973
2	0.769	0.761	0.902	0.898
3	0.874	0.849	0.960	0.939
4	0.907	0.820	0.964	0.945
5	0.917	0.917	0.964	0.964
6	0.806	0.804	0.850	0.848
7	0.963	0.957	0.989	0.987
8	0.979	0.897	0.992	0.963
9	0.990	0.967	0.990	0.967

The HO tile energy threshold is 150 MeV (including pedestal noise and photostatistic effects). HO tile trigger bits are ORed. The HO confirmation requirement has been applied to all (only low-quality) RPC triggers. The statistical MC error of the efficiency numbers is ± 0.001 .

Table 6 should be multiplied by the RPC trigger efficiencies given in Table 2 (taken from Ref. [5]).

Another important feature of the low-quality-only requirement is the stability of the efficiencies with respect to the HO tile energy threshold. Table 7 shows the HO confirmation efficiencies for 100 GeV/ c p_T muons triggered by the RPC as a function of the RPC trigger tower number, and for the three different HO tile energy thresholds considered in Table 3. HO trigger bits are ORed within the minimal HO rapidity map. Efficiencies are remarkably stable, even for a threshold as high as 245 MeV. The reason for this behaviour is that HO confirmation is only required for $\sim 30\%$ of the muons (low-quality). This is an important feature because allows the tuning of the actual thresholds at CMS as a function of the observed noise and background conditions.

6.2. Rate reduction

As discussed at the end of Section 4, to compute the rate reduction, a threshold at which the HO occupancy is dominated by electronic noise should

Table 7

Comparison of the HO confirmation efficiencies for 100 GeV/ c muons triggered by the RPC as a function of the RPC trigger tower number, and for three different HO tile energy thresholds

RPC tower	HO efficiency		
	$E_{HO} > 150$ MeV	$E_{HO} > 200$ MeV	$E_{HO} > 245$ MeV
0	0.964	0.961	0.961
1	0.973	0.971	0.969
2	0.898	0.887	0.870
3	0.939	0.926	0.909
4	0.945	0.934	0.918
5	0.964	0.954	0.934
6	0.848	0.834	0.815
7	0.987	0.975	0.965
8	0.963	0.960	0.952
9	0.967	0.944	0.934

HO trigger bits are ORed according to the minimal HO rapidity map. The HO confirmation requirement has been applied to low-quality RPC triggers only. The statistical MC error of the efficiency numbers is ± 0.001 .

be chosen in order not to be affected by the other less accurately predictable backgrounds. At 1% occupancy, the single tile energy threshold is 150 MeV. However one has to consider that the Minimal Map includes 2 (or 3) tiles per RPC trigger tower. In order to tune for 1% trigger tower occupancy, the HO energy threshold should be increased to 165 MeV (175 MeV, respectively). The improved RPC trigger rates can be computed by simply considering a reduction factor of 100 for low-quality triggers, and nothing for high-quality triggers. Therefore, if the proportion of RPC high-quality triggers turned out to be much smaller than 1%, the HO trigger rate reduction would be fully exploited. Indeed this is the case.

We have computed the RPC trigger rates using ORCA. The parameters of the simulation were:

- trigger gate width: 20 ns,
- RPC cluster size: parameter $cs = 1.5$, i.e. average cluster size ~ 2 strips,
- RPC streamers: none,
- RPC efficiency: 100% (conservative),
- RPC noise: 50 Hz/cm²,
- neutron background: nominal rate [3],

- statistics: 110 million events, corresponding to 4.4 s of LHC.

The RPC PACT algorithm as a function of the RPC trigger tower has been specified in Section 4. We study four p_T thresholds: 0 and 5 GeV/ c (very-low-), 10 GeV/ c (low-), and 25 GeV/ c (high- p_T).

Table 8 shows a comparison of the RPC trigger rates (Hz) without and with HO confirmation as a function of the RPC trigger tower. The rates for the RPC alone are given for all triggers and for high-quality triggers. For $p_T > 10$ GeV/ c the rates obtained agree well, within statistics, with the numbers in Table 2 [5]. In the last column, the HO confirmation requirement has been applied to low-quality RPC triggers only.

The conclusion is that it can be safely assumed a full rejection factor of about 100. At very-low- p_T the RPC + HO trigger rates become now comparable to the RPC ones with $p_T > 25$ GeV/ c . Above 10 GeV/ c the HO requirement can be avoided in Towers 0–7. Even in this case the reduction factor is still 10–15. In particular, in the only problematic case from the efficiency point of view (Tower 6 at low- and high- p_T), the rates are so small anyway that the HO seems completely unnecessary.

For comparison, assuming 1.5 pe noise/bucket, the full rejection factor for the same HO energy threshold is 30. Applying HO confirmation only to Towers 8–9 for low- and high- p_T RPC triggers, the reduction is still 8–10.

7. Hardware implementation

The physical implementation of a RPC + HO combined trigger is mostly based on the existing RPC and HCAL trigger electronics. Until now, these two triggers have been designed, developed, and tested independently. The RPC + HO combined trigger implies that, in the future, the two triggers should be properly interfaced. Fortunately, this is not only possible but relatively simple. In this section the classical hardware implementations of the RPC and HO (HCAL) triggers are first reviewed. Then the modifications required for the RPC + HO trigger are discussed. The RPC and HO data flow is shown in Fig. 11.

Table 8

Comparison of the RPC trigger rates (Hz) without and with HO confirmation as a function of the RPC trigger tower, and for several p_T thresholds

RPC tower	RPC trigger (Hz)	RPC high-quality (Hz)	RPC + HO trigger (Hz)
$p_T > 0$ GeV/ c			
0–5	20872 ± 17	8.26 ± 0.19	216.9 ± 0.3
6–7	7795 ± 10	2.60 ± 0.11	80.5 ± 0.1
8	11217 ± 12	5.12 ± 0.15	117.2 ± 0.2
9	1657 ± 5	—	16.6 ± 0.1
0–9	41541 ± 24	16.0 ± 0.3	431.2 ± 0.4
$p_T > 5$ GeV/ c			
0–5	18965 ± 16	7.46 ± 0.18	197.0 ± 0.2
6–7	2434 ± 6	0.95 ± 0.07	25.3 ± 0.1
8	4905 ± 8	2.04 ± 0.10	51.1 ± 0.1
9	539 ± 3	—	5.4 ± 0.1
0–9	26843 ± 19	10.4 ± 0.3	278.8 ± 0.3
$p_T > 10$ GeV/ c			
0–5	142 ± 1	0.08 ± 0.01	1.49 ± 0.01
6–7	2.7 ± 0.1	0.005 ± 0.003	0.031 ± 0.003
8	1297 ± 4	0.49 ± 0.05	13.5 ± 0.1
9	152 ± 1	—	1.52 ± 0.01
0–9	1592 ± 5	0.58 ± 0.05	16.5 ± 0.1
$p_T > 25$ GeV/ c			
0–5	32.5 ± 0.4	0.02 ± 0.01	0.34 ± 0.01
6–7	0.84 ± 0.06	<0.005	0.008 ± 0.001
8	489 ± 3	0.17 ± 0.03	5.06 ± 0.04
9	48.7 ± 0.8	—	0.49 ± 0.01
0–9	571 ± 3	0.19 ± 0.03	5.90 ± 0.04

The rates for the RPC alone are given for all triggers and for high-quality triggers. In the last column, the HO confirmation requirement has been applied to low-quality RPC triggers only.

Signals from the RPC chambers are processed by Front End Boards [3] and delivered to the trigger system [4]. The data are transmitted through Low Voltage Differential Signal (LVDS) cables to Link Boards distributed around the CMS detector, where they are assigned a bunch crossing,

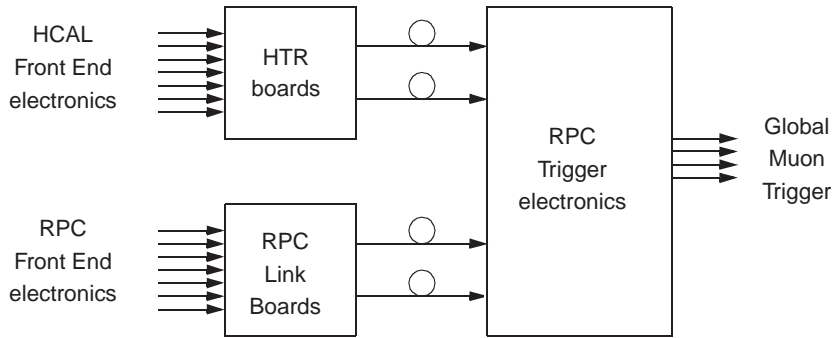


Fig. 11. RPC and HO data flow.

synchronized, compressed and multiplexed. Then they are converted to optical signals and sent through optical fibers to the RPC Trigger Crates located in the underground Counting Room. The Gigabit Optical Link (GOL) chips developed at CERN are used [12]. GOL chips can transmit up to 1.6 Gbit/s, which is equivalent to 40 bits transmitted at 40 MHz. In the Counting Room, there are 12 RPC Trigger Crates, one per logical 30° sector in ϕ . One RPC Trigger Crate contains 9 Trigger Boards, each dealing with 3 or 4 η trigger towers. At the Trigger Boards the Pattern Comparator track-finding logic is carried out.

The HO front end electronics are located on the detector. Some details of the electronics layout may be found in Ref. [13]. Signals are transmitted using GOLs (three channels per link) to 48-channel HCAL Trigger and Readout (HTR) boards located in the Counting Room. The HTR boards compute the trigger primitives which are routed to Synchronization and Link Board (SLB) mezzanine cards [14]. Each HTR board can accommodate up to 6 SLBs. The firmware in the SLB accumulates a histogram which is used to synchronize the links. Data are transmitted on Vitesse copper cables from the SLBs to the Regional Calorimeter Trigger.

Since the HO HTR boards are not used in the HCAL trigger, there is freedom to optimize the HO trigger primitives from the RPC perspective. The HO HTR boards provide energy-over-threshold trigger bits. Thresholds are programmable and can be different for different tile positions. The

HO trigger bits are organized in groups to match the RPC Trigger Board scheme, as described in Table 5.

It is also necessary to send the trigger bits using GOL for reasons of RPC compatibility. The interface between the HO and RPC will use a new version of the SLB card with optical outputs [15]. This optical SLB is the only new piece of electronics developed for the RPC+HO trigger. The design of the optical SLB is based on the Xilinx Virtex-II Pro family of FPGAs [16]. These FPGAs integrate a full-duplex RocketIO transceiver on-chip. A RocketIO cell has the following features which are useful for our application:

- Variable speed operation from 622 Mbit/s to 3.125 Gbit/s transfer rates.
- The clock synthesizer is a monolithic PLL with no external components. It provides $\times 20$ multiplication of a user-provided reference clock for the transmitter, and extracts phase and frequency from the incoming data stream for the receiver.
- The transmitter block accepts one, two or four byte characters (each 8 or 10 bits wide). A bypass-able 8B/10B encoder is provided, compatible with Gigabit Ethernet, XAUI, Fibre Channel and InfiniBand. The transmitter has a built-in four-word FIFO.
- The serializer transmits bits at the reference frequency $\times 20$ on two outputs at a programmable level, with programmable on-chip termination (50Ω or 75Ω). Four selectable pre-emphasis levels allow the transceiver to drive

up to 1 m of PCB traces with two connectors at the maximum baud rate.

A complete HO-RPC interface scheme, satisfying all constraints from both systems, has been worked out. The details, too technical to be included here, can be found in Ref. [17]. In summary, the HO Tile data are processed in 4 HO HTR boards. There are 84 different HO bit streams, transmitted via 108 optical links. At the RPC end, the HO optical links have been accommodated in the available RPC Trigger Board inputs. HO trigger bits will be treated and incorporated into the PACT like an extra RPC plane.

8. Conclusions

The conceptual design of an improved CMS RPC muon trigger using the HO scintillators has been presented. The geometrical integration, RPC+HO extended trigger algorithm, and basic lines of the hardware implementation have been established. If the HO performance obtained at the test beam could be systematically achieved at CMS, confirmation of low-quality RPC triggers would reduce the rates up to a factor 100. Even if the performance is not as good, the rate reduction factors are important enough to be considered. The efficiency of the algorithm proposed here is $\approx 90\%$, and remarkably stable as a function of the HO energy threshold. Fine tuning at CMS is therefore possible. A combined RPC+HO trigger, following the present design, is now part of the CMS Level 1 Trigger baseline.

The implications of the present rate reduction factors would be much more important if the RPC noise could be reduced to 5 Hz/cm^2 . In this case, it would be possible to consider the use of the HO to improve the efficiency, for instance, 3/6 RPC triggers confirmed by the HO. This can be used in particular in Tower 6 where there is a clear efficiency problem. Under these circumstances, 3/5 coincidences confirmed by the HO could be accepted. Yet another option to be used in the case of low RPC noise is the old “classic” 3/4 algorithm [4]. In that case the HO can again be used to reduce the rate while preserving high

efficiency. Performance of those algorithms is under study and the results will be published elsewhere.

Acknowledgements

We thank R. Alemany, D. Baden, M. Cerrada, J. Elias, J. Freeman, T. Grassi, D. Green, E. Hazen, M. Huhtinen, A. Kalinowski, A. Skuja, W. Smith, C. Tully, and P. Zotto for illuminating discussions.

References

- [1] CMS Collaboration, CMS TDR: the Hadron Calorimeter Project, CERN-LHCC-1997-031.
- [2] E. Hazen, et al., Nucl. Instr. and Meth. Phys. Res. A 511 (2003) 311.
- [3] CMS Collaboration, CMS TDR: the Muon Project, CERN-LHCC-1997-032.
- [4] CMS Collaboration, CMS TDR: the Level-1 Trigger Project, CERN-LHCC-2000-038.
- [5] A. Kalinowski, J. Krolikowski, P. Zynch, G. Wrochna, CMS NOTE-2001/045.
- [6] CMS detector simulation software group, <http://cmsdoc.cern.ch/cmsim/cmsim.html>.
- [7] T. Sjostrand, P. Eden, C. Friberg, L. Lonnblad, G. Miu, S. Mrenna, E. Norrbin, Comput. Phys. Commun. 135 (2001) 238.
- [8] H.C. Fesefeldt, Technical Report PITHA 85-02, III Physikalisches Institut der RWTH Aachen, 1985.
- [9] A. Fasso, A. Ferrari, J. Ranft, P.R. Sala, Proceedings of the Monte Carlo 2000 Conference, Lisbon, Portugal, 2000; and references therein.
- [10] M.B. Chadwick, et al., Los Alamos Report LA-UR-98-1825, Nucl. Sci. Eng. 131 (1999) 293.
- [11] CMS detector reconstruction software group, <http://cmsdoc.cern.ch/orca>.
- [12] P. Moreira, et al., Proceedings of the Seventh Workshop on Electronics for LHC Experiments, Stockholm, Sweden, 2001.
- [13] E. Hazen, J. Rohlf, S. Wu, A. Baden, T. Grassi, Proceedings of the Seventh Workshop on Electronics for LHC Experiments, Stockholm, Sweden, 2001.
- [14] J.C. DaSilva, http://joule.bu.edu/~hazen/cms_trig/SLB_PMC_spec.pdf.
- [15] Some technical details of the GOL-based SLB project may be found at http://joule.bu.edu/~hazen/cms_trig/.
- [16] The Virtex-Pro is described at <http://www.xilinx.com/products/virtex2pro/rocketio.htm>.
- [17] C. Albajar, J.F. de Trocóniz, J. Rohlf, G. Wrochna, CMS NOTE-2003/009.